Computation of accommodation coefficients and the use of velocity correlation profiles in molecular dynamics simulations

Peter Spijker,* Albert J. Markvoort, Silvia V. Nedea, and Peter A. J. Hilbers
Departments of Biomedical and Mechanical Engineering, Eindhoven University of Technology, P.O. Box 513, 5600 MB Eindhoven, The Netherlands
(Received 30 September 2009; published 22 January 2010)

For understanding the behavior of a gas close to a channel wall it is important to model the gas-wall interactions as detailed as possible. When using molecular dynamics simulations these interactions can be modeled explicitly, but the computations are time consuming. Replacing the explicit wall with a wall model reduces the computational time but the same characteristics should still remain. Elaborate wall models, such as the Maxwell-Yamamoto model or the Cercignani-Lampis model need a phenomenological parameter (the accommodation coefficient) for the description of the gas-wall interaction as an input. Therefore, computing these accommodation coefficients in a reliable way is very important. In this paper, two systems (platinum walls with either argon or xenon gas confined between them) are investigated and are used for comparison of the accommodation coefficients for the wall models and the explicit molecular dynamics simulations. Velocity correlations between incoming and outgoing particles colliding with the wall have been used to compare explicit simulations and wall models even further. Furthermore, based on these velocity correlations, a method to compute the accommodation coefficients is presented, and these newly computed accommodation coefficients are used to show improved correlation behavior for the wall models.

DOI: 10.1103/PhysRevE.81.011203 PACS number(s): 47.45.−n, 02.70.−c

I. INTRODUCTION

For the cooling of microdevices microchannels and nanochannels are widely recognized as an important application. These microdevices can be cooled locally, where the heat is produced, in a compact and efficient way by using a gas or liquid flowing through the nanochannels. Understanding the heat transfer characteristics of these nanochannels is, therefore, important. This is especially the case close to the gas-solid interface. However, in systems of microsize the underlying physics is not yet fully understood, and debate is going on whether the macroscopic laws of physics can simply be scaled down to the microscale [1]. It appears that flow transport properties can no longer be described adequately by a Navier-Stokes continuum approach, since this approach requires the size of the system being not too small and the gas not very dilute [2]. For smaller length scales, it is possible to change the governing equations of the flow model from the Navier-Stokes equations to the Boltzmann equation. Nonetheless, at sufficiently small length scales the particle behavior becomes essential and, therefore, particle simulation methods are necessary. An example of such is molecular dynamics (MD) simulations. For investigation of the gas-solid interface MD is appropriate, since this technique allows the walls to be modeled explicitly, as well as the gas-wall interaction.

Recently, several MD studies investigating the influence of the gas-solid interface interactions on the heat flow in nanochannels have been reported, in which the behavior of a gas confined between two plates is investigated [3–5]. In some of these studies MD simulations are compared with different wall models to replace the explicitly modeled walls, since the latter restrains the simulation size, due to the huge amount of computational cost. Different types of boundary conditions have been suggested over the years and used for comparison, such as replacing the explicit wall with a wall potential [5–7], or by using stochastic wall models instead.

In this paper, the stochastic wall models are discussed first, followed by a set of MD simulations of two different gas-wall systems. For each of these systems interaction parameters between the gas and the wall are determined from so-called contact angle simulations. Based on the collision data of the MD simulations, phenomenological parameters (the accommodation coefficients) can be computed and used potentially as input for the stochastic wall models. These stochastic models are then compared to the MD simulations. One of the most promising methods of comparison is the velocity correlations between the incoming and outgoing velocities of particles colliding with the wall. Finally, a method to compute accommodation coefficients based on the velocity correlations is presented and compared with the explicit wall and stochastic wall models.

II. STOCHASTIC WALL MODELS

The stochastic wall models have in common that when a gas particle collides with the solid wall; the models generate a new velocity for the reflecting particle, where this new velocity is based in a certain way on the incoming velocity [8]. The most simple conditions include the reflective and thermal wall models [9,10]. For instance, a collision is said to be purely reflective when the solid wall is perfectly smooth and there exists an infinite interaction potential with the gas particle, thus, the solid wall is a hard wall. In the event of such a collision, a particle is send back with the same, but reverted, velocity. Hence, the perpendicular component of the velocity of a particle impinging on the wall is

*Present address: EPFL, Switzerland; peter.spijker@epfl.ch

reversed, whereas the parallel components remain unchanged.

On the other hand the thermal wall model assumes that when a particle hits a rough wall it undergoes a series of collisions with the wall, and, finally, its velocity when leaving the proximity of the wall is randomized and uncorrelated with its initial velocity. The distribution of the velocities for particles leaving the wall is completely determined by the temperature of the wall. This so-called thermal wall model thus results in purely diffusive reflection. Thus, after a collision with a wall modeled by the thermal wall model a particle has no recollection whatsoever of its incoming velocity.

Both these wall models have already been proposed by Maxwell [11], but the thermal wall model has been extended more recently [9,12–14]. Apart from the two separate models, Maxwell also proposed a linear combination of the models, considering the real reflecting surfaces as an intermediate between a perfectly elastic smooth surface (reflective wall) and a perfectly absorbing surface (thermal wall) [15]. The linear combination is governed by the accommodation coefficient α, which represents the weight of the diffusion in the gas colliding with the wall, and is by definition between zero (reflective) and one (thermal). A more detailed discussion on accommodation coefficients is deferred until later in this paper. Recently, Yamamoto *et al.* adapted the Maxwell model by allowing different accommodation coefficients for the different components of the velocity [16]. In this model, each impinging particle is reflected either specularly or diffusely at the wall, where the accommodation coefficient determines the percentage of the particles being reflected in either way.

Another phenomenological model, like the above discussed Maxwell-Yamamoto model, is the model proposed by Cercignani and Lampis [8,17–19] and later extended by Lord [20–22]. This model also uses two accommodation coefficients, albeit different ones than in the case of Yamamoto's extension of the Maxwell model. As with all discussed models, the Cercignani-Lampis model treats the velocity components independently.

III. MOLECULAR DYNAMICS SIMULATIONS

One of the most studied nanochannel systems, both experimental and theoretical, is that of a noble gas (e.g., argon, xenon, or helium) confined between two metal plates (e.g., steel, platinum) [23–28]. Recently, numerical studies using particle models on similar systems have been reported both for monoatomic gases [29–35], and for diatomic molecular gases [36,37].

In order to allow for comparison with both experimental and other numerical studies the systems that are used in the MD simulations are either argon (Ar) or xenon (Xe) particles trapped between two parallel platinum (Pt) plates of different temperatures (a warm and a cold wall). In Fig. 1, a representation of such a system is depicted. Notice that in each system only argon or xenon is present between the walls, so no mixtures of these gases are examined.

The masses for argon, xenon and platinum in the MD simulations are set to 39.95, 131.3, and 195.1 amu, respectively, and the diameters for each of the three particle types

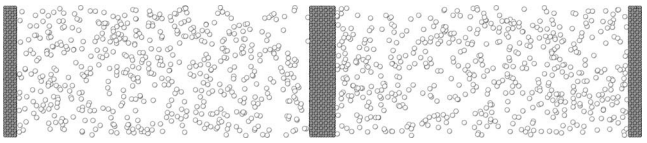

FIG. 1. An orthographic representation of the system under consideration for the MD simulations. In this case the argon particles are trapped between two parallel platinum plates, which form an FCC lattice. The central wall is the warm wall (600 K) and the outside walls are the cold walls (300 K). The dimensions of the system are $50\times10\times10$ nm, and the total number of atoms is approximately 28 000.

are set to 0.382 nm for argon, 0.441 nm for xenon, and 0.277 nm for platinum.

In both systems only nonbonded interactions are considered, which are all modeled using Lennard-Jones potentials. Based on the atomic diameters the characteristic lengths σ_{ii} for each of the atoms can readily be computed, which are 0.340 nm for argon, 0.393 nm for xenon, and 0.247 nm for platinum. Using the Lorentz-Berthelot mixing rules the characteristic lengths belonging to cross-type nonbonded interactions can be computed [38].

Based on computations using the Sutton-Chen potential, which is more applicable for metals such as platinum, a Lennard-Jones interaction strength for the platinum-platinum interaction of 19.42 kJ/mol is reported [39]. However, because this interaction strength is only derived around atmospheric conditions, using a higher interaction strength is necessary for the temperature ranges that are investigated in this paper to prevent the crystal lattice from evaporating. Therefore, an interaction strength of $\varepsilon_{\text{Pt-Pt}}=31.36$ kJ/mol is used for this interaction [16]. Due to this strong interaction strength the platinum particles form an FCC lattice, which does not melt even at higher temperatures. For the gas-gas interactions the standard interaction strengths for argon and xenon are used, which are $\varepsilon_{\text{Ar-Ar}}=0.996$ kJ/mol and $\varepsilon_{\text{Xe-Xe}}=1.834$ kJ/mol, respectively [40].

The only nonbonded interaction parameter not yet determined is the one for the gas-wall interactions, ε_{GW}. With respect to the heat transfer capabilities of the system this is the most important parameter, and, therefore, it is important to derive it accurately.

Maruyama *et al.* performed simulations of a liquid argon droplet in contact with a platinum surface in order to obtain the gas-wall interaction parameter for platinum and argon [30]. When such a liquid droplet is placed in contact with a solid surface, some degree of wetting occurs, which is determined by a force balance between adhesive and cohesive forces [41]. The angle at which the droplet interface meets the solid surface is called the contact angle. Others have used the same technique to obtain interaction parameters for water-carbon and water-silica interactions [42,43].

From a thermodynamical point of view the existence of such a contact angle (or better a contact line between the liquid, vapor, and solid interface) can be understood by assuming that the system is in equilibrium, and, thus, that the chemical potential should be equal in all phases [44]. In the case of a liquid argon droplet placed on a platinum surface,

three phases can be distinguished: a solid phase (S, the platinum wall), a liquid phase (L, the droplet), and a vapor phase (V, containing evaporated particles from the liquid droplet). For each of the three contact interfaces the free energies can be written down, which are γ_{SV}, γ_{SL}, and γ_{LV}, respectively. In equilibrium Young showed [45] that these three energies are related to each other through the contact angle,

$$\gamma_{LV} \cos \phi_0 = \gamma_{SV} - \gamma_{SL}, \tag{1}$$

where ϕ_0 is the equilibrium contact angle. Because the free-energy γ_{LV} for the liquid-vapor interface is related to the interaction parameter for the gas-gas interactions ε_{GG}, the two unknowns are γ_{SV} and γ_{SL}. However, if it is assumed that the difference $\gamma_{SV}-\gamma_{SL}$ is proportional to the gas-wall interaction parameter, Eq. (1) gives a linear relationship between the Lennard-Jones parameter ε_{GW} and the contact angle ϕ_0 [30]. It follows that a low value of the contact angle (thus, $\cos \phi_0 \approx 1$) corresponds to a high Lennard-Jones interaction parameter. However, it must be noted that surface roughness, which is eliminated from this simplified model, is known to enhance the contact angle [46]. It is debated whether this macroscopic derivation of the contact angle is applicable to the microscopic scale, where the particle size becomes important, but some studies, including this one, indicate that this is at least approximately correct [47–50].

Using different interaction strengths for the platinum-argon interaction parameter $\varepsilon_{Pt\text{-}Ar}$, Maruyama *et al.* showed different contact angles of the argon droplet with the platinum surface, which indeed formed a linear relationship [30,31]. Based on their contact angle simulations, Maruyama *et al.* decided to use a quite wettable interaction strength between platinum and argon of 0.538 kJ/mol. In their paper they used as characteristic length $\sigma_{Pt\text{-}Ar}$ for the platinum-argon interaction 0.309 nm, whereas according to our calculations this should be 0.294 nm. The difference arises due to a different computation of the nearest neighbor in the platinum crystal lattice. Maruyama *et al.* mention that in their platinum crystal the nearest neighbors are at 0.277 nm, which they use as Lennard-Jones parameter $\sigma_{Pt\text{-}Pt}$. However, in a crystal lattice the nearest neighbor is found around the distance $\sqrt[6]{2}\sigma_{Pt\text{-}Pt}$. Thus, computing $\sigma_{Pt\text{-}Ar}$ using the Lorentz-Berthelot mixing rules leads to a different value for $\sigma_{Pt\text{-}Ar}$.

Therefore, to re-parameterize the gas-wall interaction parameter between platinum and argon new simulations similar to those by Maruyama *et al.* need to be performed. Moreover, because Maruyama *et al.* only investigated platinum and argon, these simulations have to be repeated in the case of xenon and platinum as well. For both argon and xenon the same simulation protocol is followed.

In this protocol, first a liquid droplet of the gas is formed by cooling down randomly placed gas atoms from 300 K to a temperature within the range belonging to the liquid phase (which is 85 K for argon and 163 K for xenon, respectively). From each of these simulations the formed droplet is extracted, dismissing any gas atoms in the vapor phase surrounding the droplet. In the case of argon, this leads to a droplet consisting of 2535 atoms (with an approximate diameter of 6 nm), and for xenon to a droplet with 2338 atoms (approximately 7 nm in diameter). Each of the droplets is then placed in the proximity of a platinum solid wall of 20×20 nm^2 and 10 layers thick. In the direction perpendicular to the wall, the simulation box extended for at least 10 nm ensuring that the droplet does not interact with the periodic image of the platinum wall.

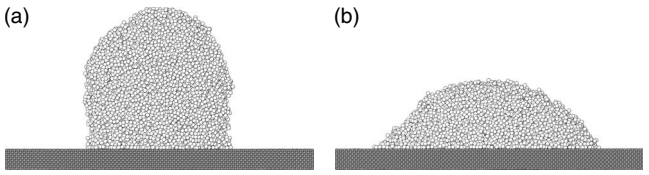

FIG. 2. Two snapshots from the contact angle simulations for an argon droplet near a platinum wall. In this simulation the interaction parameter $\varepsilon_{Pt\text{-}Ar}$ equals 0.6 kJ/mol. In (a) the system is shown as it is around 40 ps after the start of the simulation, and in (b) the same system but now around 300 ps. For clarity the vapor is omitted from the snapshots.

Subsequently, for each of the two gases a series of MD simulations are performed at the same temperatures as mentioned previously, with different Lennard-Jones parameters for the gas-wall interaction strength, while keeping all other parameters fixed. In the case of argon the range for $\varepsilon_{Pt\text{-}Ar}$ extends from 0.20 to 0.75 kJ/mol and for xenon the range of $\varepsilon_{Pt\text{-}Xe}$ is from 0.20 to 1.15 kJ/mol. In both cases the interaction parameters are changed with steps of 0.05 kJ/mol each time.

Depending on the interaction parameter the droplet exhibits different wetting behavior. In Fig. 2, two snapshots for the argon simulation with $\varepsilon_{Pt\text{-}Ar}=0.6$ kJ/mol are shown, one from the beginning of the simulation (around 40 ps) and the other toward the end of the simulation (around 300 ps). The simulations are stopped when the droplet reaches equilibrium, i.e., its shape does not change anymore.

From each simulation density profiles for the final configuration are computed, which are constructed in the r,ϕ plane, with the axis normal to the platinum surface going through the center of mass of the droplet. These radial density profiles allow for the contact angle to be computed by fitting a circle through the liquid-vapor interface and to determine the angle between this circle and the platinum wall, see Fig. 3(a).

The computations of the radial density profiles are influenced by the choice of an appropriate bin size, which lead to different contact angles. In order to reduce errors due to the choice of the bin size, six different bin sizes are used to compute the contact angles and each of these are treated as different and independent contact angle measurements. Thus, for each MD simulation with a different gas-wall interaction parameter, six contact angles are measured, which allow for an average contact angle to be computed along with its variance.

In Fig. 3(b) the relation between the cosine of the contact angles and the gas-wall interaction parameter is shown. For both argon and xenon it is clear that there exists a linear relationship, which is stressed even more by performing a least-squares linear fit through all measured contact angles for each gas (giving regression coefficients of 0.96 and 0.97, respectively). The deviations from the linear fit for small

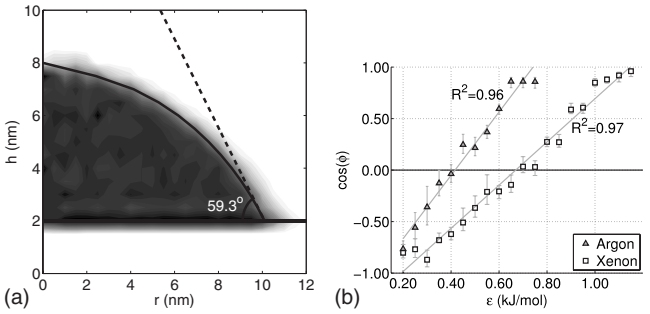

FIG. 3. In (a) the radial density profile for an argon droplet on a platinum surface is shown, which is used to compute the contact angle belonging to the Lennard-Jones interaction parameter $\varepsilon_{\text{Pt-Ar}}=0.6$ kJ/mol. The horizontal line indicates the first layer of the platinum wall and the circle approximates the argon droplet. The contact angle is the angle between the horizontal and the tangent line of the circle at the contact point (dashed). In (b) the relation between the Lennard-Jones interaction parameter and the cosine of the contact angle is shown for both argon and xenon. The bars denote the standard deviation found for a specific contact angle (see text). The linear least square fits including their regression coefficients are also shown.

contact angles (so $\cos\phi_0$ is close to one) are caused by the fact that determining the contact angle is difficult when the droplet is almost flat. Thus, these simulations indicate that Young's relation of Eq. (1) is valid even at the nanoscale.

Although there is now a clear relationship between the wettability character of the gas and the interaction parameter of the Lennard-Jones potential, the choice of the parameters is still to be made. Because experiments on the same systems as used in the simulations are nonexisting, this choice cannot be confirmed on an empirical basis. Maruyama *et al.* choose to use a quite wettable parameter for argon in order to prevent bubble nucleation at the platinum surface [31]. For the lack of other arguments, Maruyama's argument to prevent bubble nucleation is used to choose the Lennard-Jones interaction parameters in our systems. In Maruyama's case the quite wettable parameter coincides with a contact angle of approximately 41° ($\cos\phi_0=0.75$). Using this contact angle the interaction parameters between platinum and argon or xenon can be deduced from Fig. 3(b), which gives for $\varepsilon_{\text{Pt-Ar}}=0.6580$ kJ/mol and for $\varepsilon_{\text{Pt-Xe}}=1.0235$ kJ/mol.

A. Simulation details

As mentioned previously in the system that is investigated gas particles are trapped between two platinum walls at different temperatures. Each of the platinum walls consists of 13 520 atoms equally divided across the 10 layers of the FCC-lattice. The lattice is only sustained by the Lennard-Jones interactions between the platinum atoms. The centers of the walls are separated by a distance of 25 nm, and both walls extend approximately 10 nm in the other two directions, but due to periodic boundary conditions, the plates are in fact infinitely large. Between each of the two plates 650 gas atoms are present, resulting in a particle density of 0.26 nm^{-3} for each of the two channels. In order to take advantage of the periodic boundary conditions in the direction perpendicular to the wall, always two channels are modeled at once, one with the cold wall on the left side and with the hot wall on the right side, and vice versa for the second channel, see Fig. 1.

Based on the particle density and geometry of the system the Knudsen number, which is a measure of the rarefaction of the gas, can be computed. The Knudsen number is defined as the ratio between the mean-free path λ of the atoms and the characteristic dimension L of the system. In dilute systems, the mean free path of atoms is given by $\lambda=(\sqrt{2}\pi d^2 n)^{-1}$, where d is the particle diameter and n the number density, which equals the ratio of the number of particles N and the volume V. Furthermore, the volume in the system under investigation is $V=AL$, where A is the surface area of the platinum walls and L the distance between the walls, being the characteristic dimension of the system. Thus, the equation of the Knudsen number reduces to $\text{Kn}=A/(\sqrt{2}\pi d^2 N)$. Based on the parameters and dimensions of the two types of systems the Knudsen numbers can be computed, which are 0.24 for argon and 0.18 for xenon, respectively. Because the Knudsen numbers are of the order 10^{-1}, the continuum description is obsolete, justifying the usage of MD simulation to describe this kind of systems [1].

In the MD simulations of the nanochannels the temperatures of both walls are controlled by coupling each of the walls separately to an external heat bath, which are both controlled by Berendsen thermostats. One wall always remains at 300 K, whereas the temperature of the other wall is chosen from 150, 300, 360, 450, 600, or 1200 K. Collisions of gas particles with either wall heats up or cools down the gas, thus leading to a heat flow in the gas. Initially the gas particles are set to have an average temperature, which is exactly in between the two wall temperatures. It should be noted that the gas particles are not coupled to an external heat bath, and that their temperature change is caused only by collisions with other particles (wall or gas). The pressure in the system is kept at 1 bar using the Berendsen barostat.

Each simulation consists of two parts. In the first part the system is run until equilibrium is reached, whereas the second part is used as a production run: typically over several million time steps (with a time step size of 2 fs). For both systems equilibrium is always achieved within 1 ns (using the same time step size), thus the production run is started after the first 1 ns of simulation. Because the total number of particles in the system is about 28 000 all simulations are performed on multiple processors, but it still takes about 15 h to compute a 1 ns trajectory on six processors.

B. Tracking of collisions

During the production run part of the simulations, the gas particles that collide with either wall (cold or warm) have been traced. In the case of a hard wall, a collision is well defined, but when the wall is modeled explicitly using interaction potentials, such a collision is less well defined. Therefore, for every particle moving toward the wall which crosses a virtual border, its three velocity components are logged. When the particle crosses the virtual border again, this time moving away from the wall, its velocity components are

logged again. This event of crossing the virtual border is now called a collision. Thus, for every particle colliding with the wall, its incoming and outgoing velocity components are known, and, consequently, also is the change in kinetic energy due to the collision with the wall. Due to the low density of the system, gas-gas interactions near the wall are infrequent, but if they occur, they are included as a gas-wall interaction. Moreover, the residence time of the collision (the time between the first and the last logging) is recorded as well. The location of the virtual border is important and is determined by two factors. First the virtual border has to be far enough away from the wall in order to prevent particles still to be influenced by the wall, i.e., the interaction potential equals zero at this distance. Second, the upper limit for the location of the virtual border is determined by the mean free path of the gas particles.

The first restriction requests the virtual border to be located at least at the truncation point of the Lennard-Jones potential for the gas-wall interaction, which equals 0.734 nm for argon and 0.916 nm for xenon. Although the mean free path gives the average distance a gas particle can travel before it collides with another gas particle, collisions between particles can occur after traveling a much shorter distance. Therefore, to prevent gas-gas interactions to influence the result of the collision, the virtual border is placed at exactly the truncation point of the potential. The number of collisions recorded at one wall depends on the temperature of the system, but is typically around 100 000 for 10 ns of simulation (production run) at the current particle density.

IV. COMPUTING ACCOMMODATION COEFFICIENTS

When gas particles collide with a surface, they exchange heat. In other words, the velocity of the gas particle is changed by the collision with the wall in such a way that, on average, the temperature of the gas is closer to the temperature of the wall. A phenomenological parameter that describes the amount of adaptation to the wall temperature is the so-called accommodation coefficient, which has been previously introduced.

When the different stochastic wall models have been introduced previously, it is mentioned that several types of accommodation coefficients are necessary for each of these models, which can be computed in different ways. For instance one of the methods to compute the accommodation coefficient is to look at the temperature gradient across a nanochannel and split the contributions for particles moving toward and away from the wall [51]. One can then deduce a temperature for incoming and outgoing particles and, when compared to the wall temperature, this gives an accommodation coefficient. Another approach is to look at the velocity change upon collision, and to compute the accommodation coefficient based on the average incoming and outgoing velocities, and on the expected average velocity belonging to the wall with a specific temperature [16]. In the latter approach it is also possible to look at energies or heat fluxes instead of velocities only.

Accommodation coefficients are very sensitive to many gas and surface conditions, and, consequently, the method to compute the accommodation coefficient is very important [34]. Regardless of either method described above, the general form of the equation for both methods that gives the accommodation coefficient is

$$\alpha_\kappa = \frac{\langle \kappa_I \rangle - \langle \kappa_O \rangle}{\langle \kappa_I \rangle - \langle \kappa_T \rangle}, \tag{2}$$

where κ can be any quantity, such as the velocity in the parallel direction or the total energy. The brackets denote that the average values for these quantities need to be computed, and the subscripts denote whether the average value is to be computed from the incoming (I) particles, the outgoing (O) particles, or from the thermal wall distribution (T).

TABLE I. Based on the equations for the thermal wall it is possible to compute the expected values for several observables, e.g., the velocity or the energy. As mentioned in the text the expected values for the energy are proportional to their expected values for specific velocities, apart from some constants. Therefore, in this table, only the expected values for specific velocity types are shown.

Direction	Velocity	Energy
Parallel	$\langle v_x \rangle = 0$	$\langle v_x^2 \rangle = \frac{k_B T}{m}$
Perpendicular	$\langle v_z \rangle = \frac{\sqrt{\pi}}{2}\sqrt{\frac{2k_B T}{m}}$	$\langle v_z^2 \rangle = \frac{2k_B T}{m}$
Total	$\langle v \rangle = \frac{3\sqrt{\pi}}{4}\sqrt{\frac{2k_B T}{m}}$	$\langle v^2 \rangle = \frac{4k_B T}{m}$

Using the recorded velocity components of the collisions at one of the walls in the MD simulation it is possible to compute an accommodation coefficient belonging to that wall in that specific system. For instance, in the case of the simulation with argon trapped between two platinum walls (one at 300 K and the other at 600 K), the perpendicular velocity accommodation coefficient for the wall at 300 K can be computed using Eq. (2), where κ is replaced by v_z.

Although the MD simulations provide values for $\langle \kappa_I \rangle$ and $\langle \kappa_O \rangle$, the value for $\langle \kappa_T \rangle$ needs to be computed from the thermal wall distribution [52]. In Table I, several expected values (for the velocity and energy) for the thermal wall distribution are listed. These values can immediately be used in Eq. (2) to compute the accommodation coefficient.

The accuracy at which the accommodation coefficient is known depends on the accuracy at which the expected values for specific quantities are measured. Thus, it is important to have sufficient independent measurements to allow for an accurate computation of the expected values. In the case of the tracking of the collisions in the MD simulations, this accuracy is determined by the number of collisions that are recorded.

In order to know how many collisions allow for sufficient statistical accuracy one MD simulation of 100 ns time span is performed. In this simulation one wall is at 300 K and the other at 1200 K. During these 100 ns a total of approximately 1 million collisions per wall is recorded. Using Eq. (2) first the accommodation coefficient is computed if only one collision is taken into account, followed by taking two collisions into account, and so on until all collisions are

TABLE II. Accommodation coefficients for different gas-wall systems (shown as blocks of two rows). The system with both walls at 300 K is omitted from this table as explained in the text. The first column indicates the temperature of the wall. The next four columns give the accommodation coefficient for the three velocity components and the absolute velocity. The last four columns give the accommodation coefficient for the three energy components and the total energy. Between the brackets the standard deviation for each computed value is given.

	Accommodation coefficients for Pt-Ar							
T (K)	α_{v_x}	α_{v_y}	α_{v_z}	α_v	α_{E_x}	α_{E_y}	α_{E_z}	α_E
150	0.71 (0.00)	0.70 (0.00)	0.47 (0.02)	0.41 (0.02)	0.34 (0.03)	0.34 (0.04)	0.50 (0.02)	0.43 (0.02)
300	0.61 (0.00)	0.60 (0.01)	0.47 (0.01)	0.40 (0.01)	0.28 (0.03)	0.28 (0.02)	0.46 (0.01)	0.37 (0.01)
300	0.55 (0.01)	0.55 (0.00)	0.45 (0.12)	0.35 (0.11)	0.21 (0.31)	0.26 (0.11)	0.46 (0.10)	0.35 (0.11)
360	0.52 (0.01)	0.53 (0.01)	0.46 (0.11)	0.36 (0.08)	0.22 (0.08)	0.21 (0.11)	0.46 (0.10)	0.35 (0.07)
300	0.53 (0.01)	0.53 (0.01)	0.43 (0.03)	0.34 (0.03)	0.24 (0.06)	0.22 (0.07)	0.45 (0.04)	0.35 (0.04)
450	0.49 (0.01)	0.49 (0.00)	0.44 (0.03)	0.34 (0.02)	0.21 (0.03)	0.19 (0.04)	0.44 (0.04)	0.32 (0.02)
300	0.50 (0.00)	0.51 (0.00)	0.40 (0.02)	0.31 (0.01)	0.21 (0.03)	0.22 (0.02)	0.44 (0.02)	0.33 (0.01)
600	0.45 (0.01)	0.44 (0.01)	0.43 (0.02)	0.32 (0.01)	0.17 (0.03)	0.19 (0.02)	0.42 (0.01)	0.30 (0.01)
300	0.46 (0.01)	0.46 (0.01)	0.36 (0.01)	0.27 (0.02)	0.19 (0.02)	0.19 (0.03)	0.42 (0.01)	0.31 (0.02)
1200	0.40 (0.00)	0.40 (0.01)	0.44 (0.01)	0.32 (0.02)	0.17 (0.02)	0.17 (0.03)	0.42 (0.01)	0.29 (0.02)
	Accommodation coefficients for Pt-Xe							
T (K)	α_{v_x}	α_{v_y}	α_{v_z}	α_v	α_{E_x}	α_{E_y}	α_{E_z}	α_E
150	0.90 (0.01)	0.90 (0.00)	0.50 (0.11)	0.50 (0.12)	0.54 (0.15)	0.55 (0.17)	0.62 (0.07)	0.59 (0.09)
300	0.67 (0.02)	0.67 (0.01)	0.61 (0.03)	0.54 (0.02)	0.40 (0.05)	0.42 (0.04)	0.60 (0.03)	0.51 (0.02)
300	0.65 (0.00)	0.65 (0.01)	0.55 (0.03)	0.45 (0.02)	0.34 (0.08)	0.33 (0.07)	0.59 (0.02)	0.47 (0.02)
450	0.56 (0.01)	0.55 (0.01)	0.54 (0.04)	0.43 (0.04)	0.27 (0.09)	0.30 (0.07)	0.55 (0.03)	0.43 (0.04)
300	0.64 (0.01)	0.64 (0.00)	0.53 (0.02)	0.44 (0.01)	0.36 (0.03)	0.34 (0.04)	0.57 (0.02)	0.46 (0.01)
600	0.49 (0.01)	0.50 (0.01)	0.56 (0.02)	0.43 (0.02)	0.27 (0.04)	0.25 (0.04)	0.56 (0.02)	0.42 (0.02)

taken into account. It is observed that when at least more than 100 000 collisions are taken into account, the computation of the accommodation coefficients is always accurate enough. When the accommodation coefficients are computed for the velocity components only, the value with acceptable accuracy is already reached when around 30 000 collisions are taken into account. Because the MD simulations typically span several tens of nanoseconds, enough collisions are present to compute the accommodation coefficients accurately.

To facilitate better error estimation when computing accommodation coefficients, the set of recorded collisions for one wall from a specific system is divided into several subsets of equal size, and for each of these subsets the average incoming and outgoing velocities are subsequently computed. These averaged velocities are then used together to compute the overall average velocities. Mathematically this trick does not change the value for average velocities, but based on the intermediate average velocities it is possible to compute a standard deviation for that specific velocity. For instance, if the average incoming velocity in the perpendicular direction of one subset is denoted by $\bar{v}_z$, then the average value for the entire set is given by $\langle v_z\rangle = \frac{1}{M}\Sigma \bar{v}_z^i$, where the sum is over all M subsets and where i denotes a specific subset. The standard deviation of this velocity component Δv_z is then given by $\Delta v_z^2 = \frac{1}{M}\Sigma(\bar{v}_z^i - \langle v_z\rangle)^2$. Having the standard deviation for all velocity and energy components κ allows, following the form of Eq. (2), to compute the standard deviation for the accommodation coefficient ($\Delta\alpha_\kappa$) as follows:

$$\Delta\alpha_\kappa = \frac{|\langle\kappa_O\rangle - \langle\kappa_T\rangle|\Delta\kappa_I + |\langle\kappa_I\rangle - \langle\kappa_T\rangle|\Delta\kappa_O}{(\langle\kappa_I\rangle - \langle\kappa_T\rangle)^2}. \tag{3}$$

Using the above method to compute both the average and standard deviation for the accommodation coefficients, eight different accommodation coefficients are computed for each wall in all platinum-argon and platinum-xenon simulations. These eight accommodation coefficients are for the three velocity components (α_{v_x}, α_{v_y}, and α_{v_z}), the total velocity (α_v), the three energy components (α_{E_x}, α_{E_y}, and α_{E_z}), and the total energy (α_E). In Table II, a complete overview for all computed accommodation coefficients can be found.

This table shows several interesting phenomena, for instance, when the overall temperature of the system increases (i.e., when the warm wall gets hotter), all of the accommodation coefficients decrease. Furthermore, the colder wall in each simulation always has a higher accommodation coeffi-

cient than the warm wall. The differences between all types of accommodation coefficients for each wall temperature are also consistent throughout all simulations. Thus, the accommodation coefficients for the parallel velocity components are always larger than the accommodation coefficient for the perpendicular velocity, which is again larger than the accommodation coefficient for the total velocity. With the energies, the highest accommodation coefficient is always found for the perpendicular component of energy, while the accommodation coefficient of the parallel components of the energy this time have the lowest values. The only deviations are found for the accommodation coefficient of the perpendicular velocity with the higher temperature ranges (600 K for xenon and 1200 K for argon). It can also be observed that on average the accommodation coefficients based on the energy are lower than for those based on the velocities. The overall standard deviations for the accommodation coefficients are low, except when the two wall temperatures are close to each other (e.g., for argon when the warm wall is at 360 K), and for the platinum-xenon case with the lowest wall temperature (150 K).

The only simulations that are omitted from Table II are the simulations where both walls have the same temperature (300 K in this case). The main reason for this is that it is then impossible to compute an accurate accommodation coefficient using Eq. (2), because the denominator is almost zero when the temperature of the gas (i.e., $\langle \kappa_I \rangle$) is close to the thermal equilibrium (i.e., $\langle \kappa_T \rangle$). The same phenomenon also causes the higher standard deviations when the wall for the platinum-argon system is at 360 K, because the denominator is then near zero. This immediately shows that it is not possible, using Eq. (2), to compute the accommodation coefficients for a system with no heat flow, i.e., with two walls at almost the same temperature.

The main difference between the argon and xenon accommodation coefficients (those of xenon being higher on average) is due to the higher interaction strength with platinum for xenon. This allows for stronger attraction of xenon particles to the platinum wall and, thus, more energy transfer, giving rise to higher accommodation coefficients. For the lowest temperature (150 K) this even caused xenon atoms to stick to the wall for a long period of time, forming a layer on top of the platinum wall. Other xenon particles now collide with the liquid xenon layer rather than with the wall, but are still counted as collisions with the wall, leading to more erratic reflection causing the higher standard deviations. Simulations for the same system with the gas-gas interaction set to zero (i.e., the case of free molecular flow), showed this standard deviation to return to its normal values, indicating that the condensation of xenon indeed caused the higher standard deviations.

V. WALL MODEL SIMULATIONS

Previously, four different stochastic wall models have been discussed. These models can be implemented as boundary conditions in the MD simulations to replace the solid platinum wall, and new simulations can be performed. However, due to the different boundary conditions a different behavior for the gas is to be expected. The systems eventually will reach thermal equilibrium, but this is not necessarily the same type of thermal equilibrium as for the same system modeled using explicit platinum walls. Comparison of the wall models with the explicit solid wall is then not straightforward.

A better method is to use the recorded incoming velocities from the MD simulations as input for the wall models and to compute the new outgoing velocities accordingly. The advantage in the comparison with the explicit wall simulations is that in this case the same incoming distributions of velocities are used. Because the number of recorded collisions in the MD simulations is large, i.e., the incoming velocity distributions are smooth, accurate outgoing velocity distributions can be computed for each wall model.

However, in order to compute the new velocities for the Maxwell-Yamamoto model and the Cercignani-Lampis model, some accommodation coefficients are needed as input parameters for these models. In the case of the Maxwell-Yamamoto model, these parameters are the accommodation coefficient for the perpendicular velocity component α_{v_z} and the accommodation coefficient for the total energy α_E. With the Cercignani-Lampis model, the accommodation coefficient for the parallel velocity α_{v_x} and for the perpendicular component of the energy α_{E_z} are needed. For each wall in each different simulation these values can be obtained from Table II.

Thus, for all types of systems that have been examined using the MD simulations with the explicit platinum wall, the new outgoing velocities have been computed for all four stochastic wall models. Subsequently it is possible to compute the accommodation coefficients using the similar procedure as with the explicit platinum walls.

Obviously, the accommodation coefficients in the case of the reflective or thermal wall are all, respectively, zero or one, but this is not necessarily the case for the accommodation coefficients for the Maxwell-Yamamoto model and Cercignani-Lampis model. In Table III, accommodation coefficients for the Maxwell-Yamamoto model and Cercignani-Lampis model are shown for argon and platinum walls at 150, 300, and 600 K.

Comparing the results for the Maxwell-Yamamoto model and the Cercignani-Lampis model with the results for the explicitly modeled platinum walls shows that the accommodation coefficients are not the same for the two wall models and are also different from the computed accommodation coefficients for the explicit walls. Only the accommodation coefficients for the parallel velocity components computed from the Cercignani-Lampis model and the accommodation coefficients for the perpendicular velocity component from the Maxwell-Yamamoto model are the same as those computed from the explicit walls.

It is interesting to see whether the accommodation coefficients are recovered that have been used as input parameters for the two models. It can be seen that whenever an accommodation coefficient based on a parallel velocity component is used in a model, this accommodation coefficient is recovered. However, this is not the case for the accommodation coefficients based on energy components. Apparently,

TABLE III. Examples of accommodation coefficients for two different platinum-argon systems with the boundaries modeled by the Maxwell-Yamamoto model and the Cercignani-Lampis model, with the input accommodation coefficients obtained from Table II. The same legend for the table is used as with Table II.

	Accommodation coefficients for the Maxwell-Yamamoto model							
T (K)	α_{v_x}	α_{v_y}	α_{v_z}	α_v	α_{E_x}	α_{E_y}	α_{E_z}	α_E
150	0.43 (0.01)	0.43 (0.01)	0.46 (0.01)	0.43 (0.01)	0.42 (0.02)	0.41 (0.03)	0.46 (0.02)	0.44 (0.01)
300	0.37 (0.00)	0.37 (0.01)	0.48 (0.02)	0.43 (0.01)	0.36 (0.03)	0.36 (0.03)	0.48 (0.02)	0.42 (0.01)
300	0.33 (0.00)	0.33 (0.00)	0.40 (0.02)	0.36 (0.01)	0.33 (0.01)	0.33 (0.01)	0.40 (0.02)	0.37 (0.01)
600	0.30 (0.01)	0.30 (0.01)	0.44 (0.01)	0.38 (0.01)	0.30 (0.03)	0.30 (0.01)	0.44 (0.01)	0.37 (0.01)
	Accommodation coefficients for the Cercignani-Lampis model							
T (K)	α_{v_x}	α_{v_y}	α_{v_z}	α_v	α_{E_x}	α_{E_y}	α_{E_z}	α_E
150	0.71 (0.00)	0.70 (0.01)	0.36 (0.02)	0.61 (0.01)	0.90 (0.01)	0.91 (0.01)	0.38 (0.02)	0.63 (0.01)
300	0.61 (0.01)	0.60 (0.01)	0.24 (0.02)	0.55 (0.01)	0.87 (0.02)	0.83 (0.03)	0.24 (0.02)	0.54 (0.01)
300	0.50 (0.00)	0.51 (0.00)	0.24 (0.02)	0.48 (0.01)	0.75 (0.01)	0.76 (0.01)	0.25 (0.02)	0.49 (0.01)
600	0.46 (0.01)	0.44 (0.00)	0.12 (0.03)	0.42 (0.01)	0.69 (0.02)	0.69 (0.01)	0.13 (0.02)	0.40 (0.01)

neither of the two models generates the correct distribution for the energy components, nor does it for the perpendicular and total velocity distributions.

VI. VELOCITY CORRELATIONS

Besides the computation of the accommodation coefficients using the recorded incoming and outgoing velocities upon a collision with the wall, it is also possible to look at the incoming and outgoing velocity distributions [16,53,54]. Moreover, this also allows for a new, more extensive, way of comparison between the explicit walls and stochastic walls models, because the same recorded velocities allow to investigate the correlation between incoming and outgoing velocities. To emphasize the power of this new comparison method the systems with the warm walls at 150 and 300 K are used as an example.

These correlations between incoming and outgoing velocities can be depicted as a two dimensional probability distribution profile, which gives for a specific incoming velocity the distribution of outgoing velocities. Such correlation profiles can be constructed for each velocity component or for the total velocity.

In the case of the reflective wall model, a strong correlation is to be expected between incoming and outgoing velocities, since particles are reflected with the same velocity, only the direction is reversed. In a correlation profile this shows up as a diagonal line. On the other hand, because the thermal wall model applies diffusive reflection, no correlation is expected at all, which can be seen in a correlation profile as a two-dimensional Gaussian probability density function. Because both the reflective and the thermal wall describe the wall reflection in the limits of pure reflective or pure diffusive behavior, the results from other wall models as well as explicitly modeled walls are expected to be in between these two extremes.

In Fig. 4 the velocity correlation profiles for the platinum-argon system with the wall at 150 K are shown for all wall models discussed in this paper. In this figure, the first column gives the correlation for the parallel component of the velocity, the second column for the perpendicular component, whereas the third column gives the correlation for the absolute velocity. It has to be mentioned that in the case of the perpendicular velocity components both the incoming and outgoing velocity are given a positive value for clarity in the figure (because the velocity is reversed upon collision, the incoming and outgoing velocities should have an opposite sign). In all velocity correlation profiles the dashed lines indicate the cases for perfect reflection (diagonal) and perfect diffusion (horizontal) for a wall with a temperature of 150 K. Finally, the last column gives the distributions of the outgoing velocities (both the perpendicular and parallel component, solid lines) in comparison with the same distributions obtained from the MD simulation (dashed). On the first row the results from the simulation with explicit modeled walls are shown, followed by the results for the reflective and thermal wall models. Thereafter, the correlations and distributions from the Maxwell-Yamamoto model and the Cercignani-Lampis model are given.

The MD simulation with explicit walls clearly shows a correlation between incoming and outgoing velocities. Furthermore, the correlation profile for the perpendicular velocity component is not symmetrical along the diagonal line, indicating that the incoming gas on average leaves the wall with a lower temperature. This is in agreement with the fact that in the simulation with one wall at 150 K the other wall is at 300 K, and particles approaching the cold wall just came from the warm wall, and, thus, should be cooled down by this wall.

The velocity correlation profiles for the reflective wall show that there is a very high correlation between incoming and outgoing velocities, which is to be expected due to the nature of the reflective wall model. On the other hand the

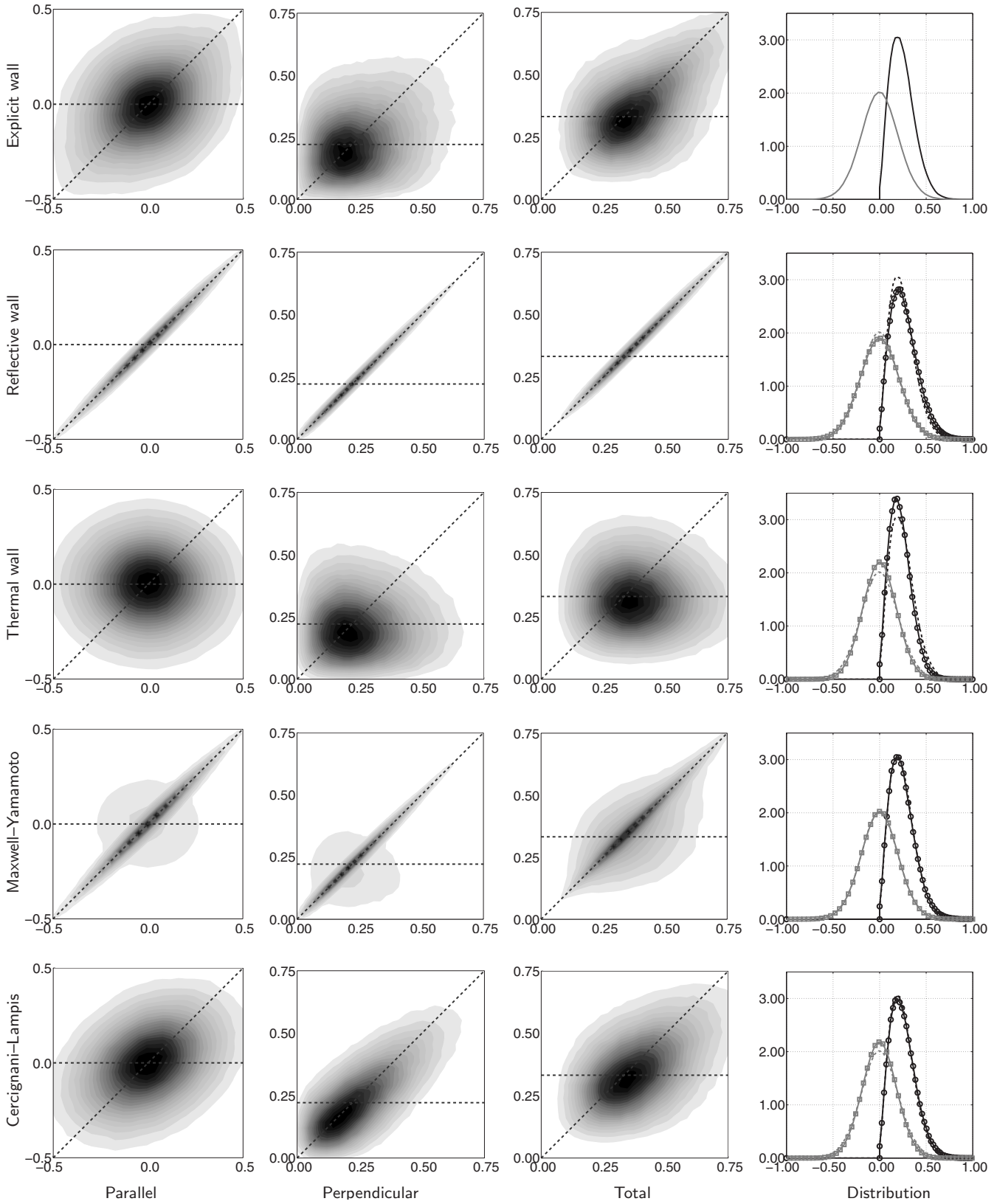

FIG. 4. Velocity correlation distributions for the 150 K wall in the platinum-argon system. These distributions are for incoming and outgoing velocities for the velocity components indicated at the bottom of each column. On the x axis always is the incoming velocity and on the y axis the outgoing velocity, both in nm/ps. The dashed lines indicate the reflective (diagonal) and thermal (horizontal) cases. In the last column the corresponding velocity distributions (perpendicular black and parallel gray) for the reflecting particles (circles) are shown in comparison with the distribution obtained from the explicit wall simulations (dashed), with the outgoing velocity on the x axis and the probability on the y axis.

thermal wall indeed shows no correlation, which can be best observed from the correlation distribution for the parallel direction. In this correlation profile the shape of the distribution is perfectly ellipsoid. If the wall would have had the same temperature as the incoming gas particles on average, the shape would be spherical. The elliptical behavior thus indicates that the thermal wall cools down the gas.

The Maxwell-Yamamoto model shows a very different correlation with respect to the explicit wall simulation. Recall from the discussion of the Maxwell-Yamamoto model that a particle is reflected either specularly or diffusively. Consequently, in the correlation profiles both the reflective and thermal wall correlation distributions can be identified.

Finally, the Cercignani-Lampis model shows better comparison with the MD simulation. Although the shapes of the distributions are not exactly the same, similar characteristics are recovered, such as the diagonal orientation of the correlation distribution for the parallel velocity components. Also the shape of the distribution for the total velocity is very similar to the distribution from the explicit wall simulation.

Turning the attention to the distribution profiles (the last column in Fig. 4), different observations can be made. All of the four wall models are in good agreement with the distributions for the explicit wall simulation, especially the Maxwell-Yamamoto model and Cercignani-Lampis model.

So, where the distribution profiles (the last column in the figure) give the impression that all wall models are in good agreement with the explicit wall simulation, it is from the velocity correlation distribution that it can be observed that only the Cercignani-Lampis model compares well with the explicit wall simulation on both analysis methods.

In Fig. 5 a similar figure is shown, but this time for the wall at 600 K. This time the comparison of correlation distributions shows a similar result as for the 150 K wall. However, the distribution for the parallel component of the Cercignani-Lampis model is far more elliptical than the shape for the same distribution in the explicit wall simulation, which is more of a diamond shape. The velocity distributions in the last column of the figure show that the reflective wall, the thermal wall, and the Cercignani-Lampis model performs less than with the wall at 150 K. Only the Maxwell-Yamamoto model always retains the same velocity distribution as the explicit wall model, but has a very poor correlation distribution comparison.

VII. VELOCITY CORRELATIONS TO COMPUTE ACCOMMODATION COEFFICIENTS

Based on the recorded velocity components of particles colliding with the wall, it is previously shown to be possible to compute accommodation coefficients with good accuracy. However, when the walls in the system both have the same temperature and the system is in thermal equilibrium, the accommodation coefficients can no longer be computed using the widely accepted Eq. (2), because division by almost zero occurs. Therefore, the general method to compute the accommodation coefficient is not always applicable.

A different method to compute the accommodation coefficients is provided by the velocity correlation profiles. As mentioned previously, in the case of a reflective wall a very strong correlation is to be expected, and no correlation at all in the case of a thermal wall (diffusive collisions). Thus, if the velocity correlation for a specific wall is close to the velocity correlation belonging to the reflective wall the accommodation coefficient is zero, whereas if the correlation is much more such as the thermal wall correlation, the accommodation coefficient is close to one.

An easy method to compute the accommodation coefficient based on this observation is to compute a line that best fits the collision data based on a least-squares approximation, and to compare this line with the diagonal (reflective collisions) and horizontal (diffusive collisions) lines from the correlation distributions. If the line has the same slope as the diagonal the accommodation coefficient is said to be zero, and when the line has the same slope as the horizontal line the accommodation coefficient is one. Consequently, the accommodation coefficient is given by $\alpha = 1 - \beta$, where β is the slope of the least-squares fitted line. In terms of the recorded incoming and outgoing quantities κ, the accommodation coefficient using this method can thus be written as

$$\alpha_\kappa = 1 - \frac{\sum_i (\kappa_I^i - \langle \kappa_I \rangle)(\kappa_O^i - \langle \kappa_O \rangle)}{\sum_i (\kappa_I^i - \langle \kappa_I \rangle)^2}, \tag{4}$$

where each sum is over all recorded collisions for that specific quantity κ. The subscripts indicate again whether the quantities belong to the I or O velocities, and the brackets indicate as usual the average values.

In Fig. 6 velocity correlation profiles for the platinum-xenon case are shown (with either the 150 or 600 K wall) together with the least-squares fitted line (solid). Also the point belonging to the average incoming and outgoing velocity is depicted (circle), through which the least-squares fitted line passes.

From this figure it can be seen that when the shape of the velocity correlation is close to the thermal wall correlation [compare Figs. 6(a) and 6(c) with the third row in Fig. 4], the least-squares line is almost horizontal. Similarly, if the least-squares line is close to the diagonal, the velocity correlation resembles the correlation from the reflective wall better [see Figs. 6(b) and the top leftmost correlation in Fig. 5].

In Table IV, an overview of the accommodation coefficients for some of the systems are shown as computed from the velocity correlations. This time the system with both walls at 300 K is included, showing that using this method, it is possible to compute an accurate accommodation coefficient for a system in thermal equilibrium.

So far only velocity correlation profiles have been constructed, but based upon the recorded incoming and outgoing velocity components it is also possible to compute energy correlation profiles. Using a similar least square fitting procedure as with the velocity correlation profiles, also accommodation coefficients for the energy can be computed, which are included in Table IV as well.

The same overall observation as with the accommodation coefficients computed using the traditional method can be

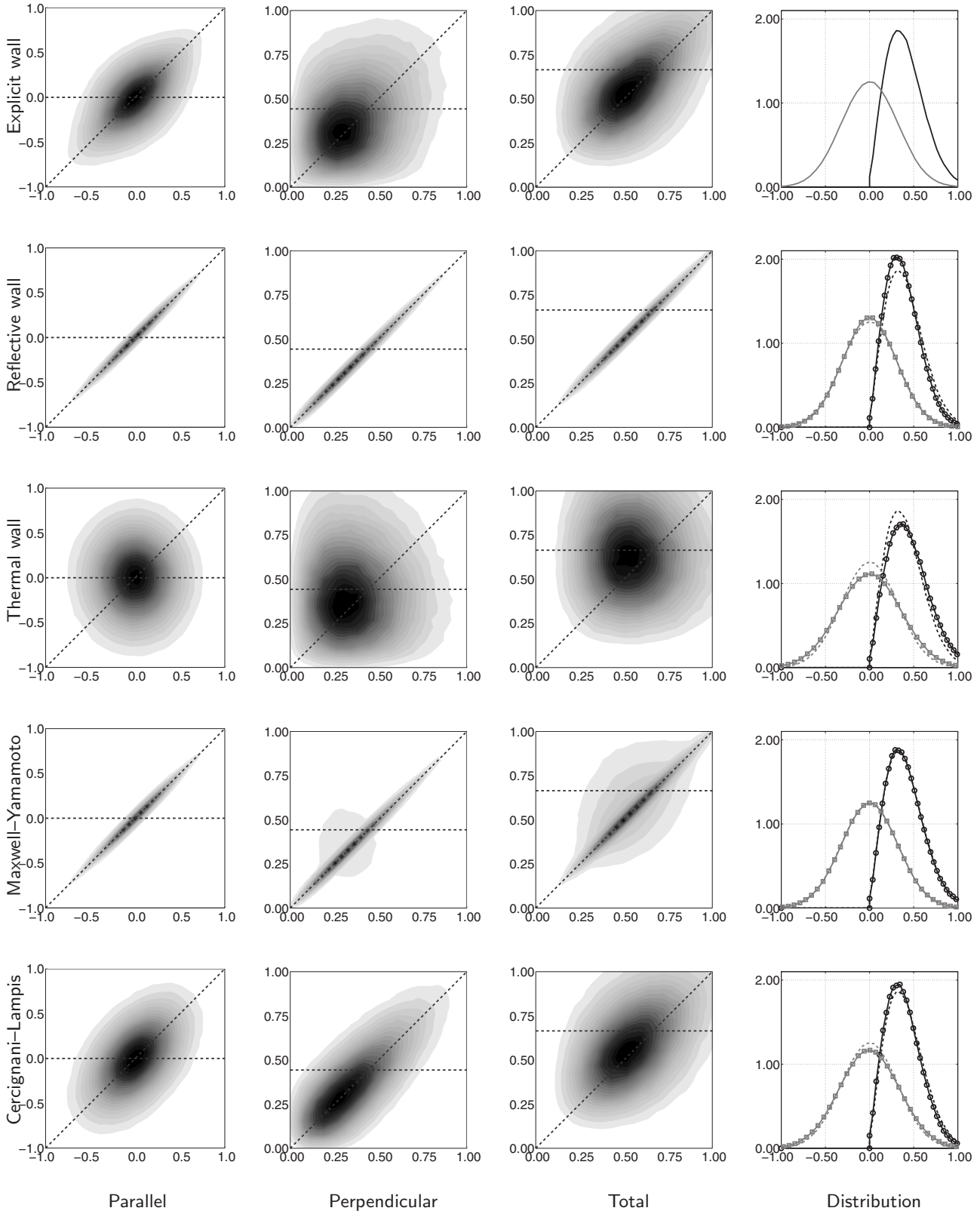

FIG. 5. Velocity correlation distributions for the 600 K wall in the platinum-argon system. These distributions are for incoming and outgoing velocities for the velocity components indicated at the bottom of each column. On the x axis always is the incoming velocity and on the y axis the outgoing velocity, both in nm/ps. The dashed lines indicate the reflective (diagonal) and thermal (horizontal) cases. In the last column the corresponding velocity distributions (perpendicular black and parallel gray) for the reflecting particles (circles) are shown in comparison with the distribution obtained from the explicit wall simulations (dashed), with the outgoing velocity on the x axis and the probability on the y axis.

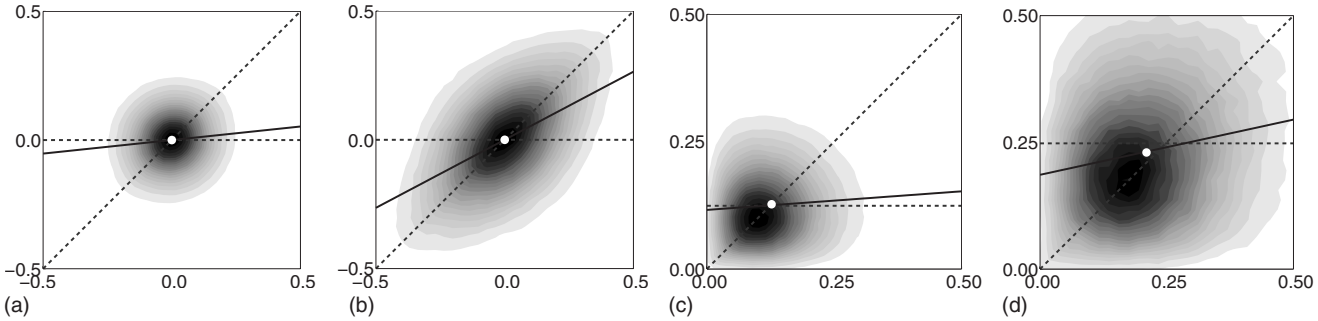

FIG. 6. Velocity correlations for the platinum-xenon system with 150 K wall (a and c) and the 600 K wall (b and d), with the incoming velocity on the *x*-axis and the outgoing velocity on the *y* axis, both in nm/ps. Both the parallel (a and b) and the perpendicular (c and d) correlation profiles are shown. In all figures the mean value for the incoming and outgoing velocities is depicted by the circle, whereas the solid line indicated the linear least square fit through all collision data.

made, e.g., the accommodation coefficient decreases when the temperature increases. However, whereas the accommodation coefficients for the parallel velocities from this table are more or less in agreement with the previously reported table, this is not the case for the accommodation coefficients for the perpendicular velocity. On general they are much higher and the decrease of the accommodation coefficient with increasing temperature is not very profound.

Previously the accommodation coefficients computed using the traditional method have been used as input for the Cercignani-Lampis model. However, also the newly computed accommodation coefficients based on the linear least squares can be used as input for the Cercignani-Lampis model. In Fig. 7 the velocity correlations for the perpendicular directions are shown for the explicit wall simulations for platinum-argon with the wall at 600 K, for the same wall using the Cercignani-Lampis model based on the original accommodation coefficients from Table II, and the Cercignani-Lampis model using the accommodation coefficients computed using the linear least-squares method.

From this figure it is clear that using the newly computed accommodation coefficients improves the velocity correlations for the perpendicular velocity considerably. Whereas, in the case of using the old accommodation coefficients the shape of the correlation is far more elliptical, the shape of the correlations for new accommodation coefficients is far more in agreement with the explicit simulations. Also, the outgoing velocity distribution in the perpendicular direction [see Fig. 7(d)] aligns almost perfectly with the distribution from the explicit wall simulation (compare with the rightmost figure on the last row of Fig. 5). Moreover, recomputing the accommodation coefficient α_{E_z} from the perpendicular velocity correlation shows that it is also in reasonable agreement with the accommodation coefficient α_{E_z} used as input (0.57

TABLE IV. An overview of different accommodation coefficients computed based on the velocity or energy correlation distributions. The legend is the same as in Tables II and III. For the simulation with both walls at 300 K only one row is included, because the walls are thermally equal.

	Accommodation coefficients for Pt-Ar							
T (K)	α_{v_x}	α_{v_y}	α_{v_z}	α_v	α_{E_x}	α_{E_y}	α_{E_z}	α_E
150	0.67	0.67	0.76	0.56	0.76	0.75	0.75	0.53
300	0.57	0.57	0.79	0.55	0.70	0.69	0.75	0.47
300	0.53	0.53	0.73	0.49	0.65	0.66	0.70	0.44
300	0.48	0.48	0.67	0.41	0.60	0.60	0.67	0.40
600	0.42	0.42	0.71	0.45	0.57	0.56	0.65	0.38
	Accommodation coefficients for Pt-Xe							
T (K)	α_{v_x}	α_{v_y}	α_{v_z}	α_v	α_{E_x}	α_{E_y}	α_{E_z}	α_E
150	0.89	0.90	0.93	0.90	0.93	0.93	0.93	0.89
300	0.64	0.64	0.87	0.71	0.76	0.76	0.83	0.65
300	0.66	0.66	0.82	0.67	0.75	0.76	0.81	0.63
300	0.61	0.61	0.78	0.62	0.71	0.72	0.78	0.61
600	0.47	0.48	0.78	0.59	0.61	0.62	0.75	0.53

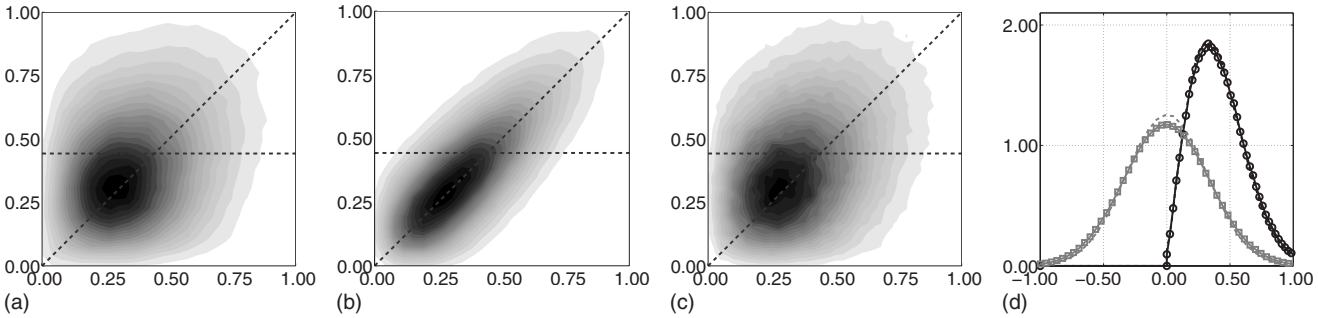

FIG. 7. In (a) the velocity correlations from the explicit wall simulation for platinum-argon at the 600 K wall is shown, and in (b) the correlations from the Cercignani-Lampis model (CL) using the accommodation coefficients computed using Eq. (2) are shown. In (c) the same correlations but now from the Cercignani-Lampis model using as input parameters the accommodation coefficients derived using the linear least-squares method, see Table IV, are shown. In all these three figures the incoming velocity is on the x axis and the outgoing velocity on the y axis, both in nm/ps. In (d) the velocity distributions (perpendicular black and parallel gray) of the Cercignani-Lampis model with the new accommodation coefficients is shown compared with the explicit wall simulations (dashed line), with the outgoing velocity on the x axis and the probability on the y axis.

vs 0.65). Thus, this method of computing the accommodation coefficients, based on the linear least square fitting procedure, does not only give better outgoing velocity distribution, but also better velocity correlation profiles.

VIII. DISCUSSION AND CONCLUSION

To remove the computational demanding solid walls from MD simulations stochastic wall models are often used. The most common stochastic wall models to encounter are (in order of complexity) the reflective wall model, the thermal wall model, the Maxwell-Yamamoto model, and the Cercignani-Lampis model. In this paper these stochastic models are compared with MD simulations using an explicitly modeled solid wall.

The two systems that have been examined with either the explicit or the stochastic walls are those of a gas (argon or xenon) trapped between two platinum walls of different temperature. In order to be able to perform the simulations a set of appropriate parameters is needed. For the gas-gas and wall-wall interactions consistent parameters are found throughout literature. However, in the case of the gas-wall interactions this is not the case. For the platinum-argon interaction, Maruyama *et al.* performed so-called contact angle simulations to use the wettability character of argon to determine an appropriate Lennard-Jones interaction parameter. Unfortunately, Maruyama made a mistake in computing the characteristic length σ belonging to the platinum-argon interaction, which leads to a different wettability behavior. Thus, to compute the interaction parameters, Maruyama's simulations are repeated with the correct characteristic length. Using the same wettability argument, Lennard-Jones interaction parameters for the platinum-argon and platinum-xenon interaction are derived. Many other researchers have used Maruyama's parameters [29,55–59], but because the difference between the current and Maruyama's platinum-argon interaction parameter is significant (0.658 kJ/mol versus 0.538 kJ/mol respectively, both based on the same wettability argument of a 41° contact angle), the results of their simulations are debatable. Although the contact angle simulations allowed to compute new Lennard-Jones interaction parameters for both platinum-argon and platinum-xenon, the lack of experimental data of similar contact angles makes it hard to justify the choice of the parameters.

It is not uncommon to encounter, as a different model to describe gas-wall interactions, a modified version of the Lennard-Jones potential, which independently scales the interaction parameter ε for the repulsive and for the attractive part of the potential [60–62]. A straightforward, but very questionable, approach to model the gas-wall interactions that is used sometimes is to get the interaction parameter ε from the Lorentz-Berthelot mixing rules [63]. Both of these different Lennard-Jones models and parameters are almost exclusively used for the platinum-argon case; different types of systems are rarely reported.

In the MD simulations with explicitly modeled platinum walls, the collisions of the gas particles with either platinum wall (which are at different temperatures) are recorded. Based on this collision data it is shown to be possible to compute the accommodation coefficients for each wall temperature in each system using the traditional relationship as given by Eq. (2). In Table II these accommodation coefficients are presented.

In their work, Yamamoto *et al.* report several different accommodation coefficients for the platinum-xenon systems [16]. Comparing their accommodation coefficients (for the same Knudsen number and temperature) with the ones from Table II shows poor agreement for all temperatures and types of accommodation coefficients. The differences are most probably due to the use of the different potential (Morse vs Lennard-Jones) with the choice of parameters discussed previously. Comparison with experimental result is difficult, because such results are almost nonexisting. Sharipov *et al.* report experimental accommodation coefficients for rarefied gas flows (including xenon and argon) in a glass tube with accommodation coefficients close to unity [64], but differences between the systems in the experiments and the simulations (glass vs platinum) make a good comparison almost impossible. Therefore, it would be very useful for the development of these models if new experiments on the systems used in this paper are performed. Moreover, from both the

experimental and the simulation side it should be tried to find a way to allow for a good comparison to measure or compute the same physical property.

Using the recorded incoming velocities from the explicit MD simulations, outgoing velocities for each of the four discussed stochastic wall models have been computed. Using the same method to compute the accommodation coefficient, it is shown that all models exert a different behavior with respect to the accommodation coefficients, and are (except for some components with the Maxwell-Yamamoto model and the Cercignani-Lampis model) also different from the explicit wall simulations. Moreover, accommodation coefficients that have been used as input in the Maxwell-Yamamoto model and the Cercignani-Lampis model are only recovered when they are based on the velocity. Thus, both models do not generate the same outgoing velocity distributions as are obtained from the explicit wall simulations.

To investigate the differences between the stochastic wall models and the explicit wall simulations, correlation profiles between incoming and outgoing velocity components are examined. From these correlation profiles it is observed that only the Cercignani-Lampis model behaves more or less similar to the explicit wall simulations. The Maxwell-Yamamoto model, which recovers the outgoing velocity distribution of the explicit wall simulations almost exactly, is on the level of the velocity correlation in strong disagreement with the explicit wall simulations. So far, many researchers only looked at the velocity distributions but not at the velocity correlations, but the results of the simulations presented in this paper, show that, in order to resemble explicit simulations best, the correlations should be taken into account when judging stochastic models on their applicability.

Because neither of the stochastic wall models matched the data from the explicit wall simulations perfectly, it has to be considered whether more elaborate models to describe the gas-wall interaction are in place. Moreover, none of the models reproduce the details of scattering revealed by molecular beam studies [54]. For instance, all of the discussed models lack the interplay between the velocity components, which could be important from the point of view of equipartition to be included. This interplay between the velocity components is most likely introduced by the roughness of the wall.

Based on the velocity correlation profiles a new method, using linear least-squares fitting, to compute accommodation coefficients has been presented. It has been shown that this accommodation coefficient corresponds in the case of the parallel velocity component to the accommodation coefficient computed using the traditional method. This correspondence can be explained due to the additive property of Gaussian distributions. Nonetheless, the new method gives different accommodation coefficients for the perpendicular velocity component as well as for the accommodation coefficients based on the energy. The method approaches the computation of the accommodation coefficient from a different perspective, and, in contrast to the traditional method, is capable of computing accommodation coefficients in the cases where both walls are at the same temperature and the system is in thermal equilibrium.

Furthermore, if the accommodation coefficients computed from the linear least-squares approach are used as input in the Cercignani-Lampis model, the velocity correlations of this model are in even better agreement with the explicit wall simulations than before. Moreover, in the new method of computing the accommodation coefficient no longer average velocities from the thermal wall case are necessary as input. This all indicates that this method of computing the accommodation coefficients is promising.

[1] S. Hardt and F. Schönfeld, *Microfluidic Technologies for Miniaturized Analysis Systems* (Springer, New York, USA, 2007).
[2] G. A. Bird, *Molecular Gas Dynamics and the Direct Simulations of Gas Flows* (Clarendon Press, Oxford, 1994).
[3] A. J. Markvoort, P. A. J. Hilbers, and S. V. Nedea, Phys. Rev. E **71**, 066702 (2005).
[4] C. Y. Soong, T. H. Yen, and P. Y. Tzeng, Phys. Rev. E **76**, 036303 (2007).
[5] P. Spijker, H. M. M. ten Eikelder, A. J. Markvoort, S. V. Nedea, and P. A. J. Hilbers, J. Mech. Eng. Sci. **222**, 855 (2008).
[6] F. F. Abraham, J. Chem. Phys. **68**, 3713 (1978).
[7] W. A. Steele, *The Interaction of Gases with Solid Surfaces* (Pergamon, New York, USA, 1974).
[8] C. Cercignani, *Rarefied Gas Dynamics: From Basic Concepts to Actual Calculations* (Cambridge University Press, Cambridge, England, 2000).
[9] A. Tenenbaum, G. Ciccotti, and R. Gallico, Phys. Rev. A **25**, 2778 (1982).
[10] R. Tehver, F. Toigo, J. Koplik, and J. R. Banavar, Phys. Rev. E **57**, R17 (1998).
[11] J. C. Maxwell, Philos. Trans. R. Soc. London, Ser. A **170**, 231 (1879).
[12] J. L. Lebowitz and H. Spohn, J. Stat. Phys. **19**, 633 (1978).
[13] M. Mareschal, E. Kestemont, F. Baras, E. Clementi, and G. Nicolis, Phys. Rev. A **35**, 3883 (1987).
[14] D. K. Bhattacharya and G. C. Lie, Phys. Rev. A **43**, 761 (1991).
[15] S. K. Dadzie and J. G. Méolans, J. Math. Phys. **45**, 1804 (2004).
[16] K. Yamamoto, H. Takeuchi, and T. Hyakutake, Phys. Fluids **18**, 046103 (2006).
[17] C. Cercignani and M. Lampis, Transp. Theory Stat. Phys. **1**, 101 (1971).
[18] C. Cercignani, Transp. Theory Stat. Phys. **2**, 27 (1972).
[19] C. Cercignani and M. Lampis, Z. Angew. Math. Phys. **23**, 713 (1972).
[20] R. G. Lord, Phys. Fluids A **3**, 706 (1991).
[21] R. G. Lord, J. Fluid Mech. **239**, 449 (1992).
[22] R. G. Lord, Phys. Fluids **7**, 1159 (1995).
[23] W. P. Teagan and G. S. Springer, Phys. Fluids **11**, 497 (1968).
[24] T. Ohwada, Phys. Fluids **8**, 2153 (1996).
[25] O. V. Sazhin, S. F. Borisov, and F. Sharipov, J. Vac. Sci. Technol. A **20**, 957 (2001).

[26] D. J. Rader, W. M. Trott, J. R. Torczynski, M. A. Gallis, J. N. Casteñeda, and T. W. Grasser, Technical Report No. 5329, Sandia National Laboratories, 2004.
[27] D. J. Rader, W. M. Trott, J. R. Torczynski, J. N. Casteñeda, and T. W. Grasser, Technical Report No. 6084, Sandia National Laboratories, 2005.
[28] W. M. Trott, D. J. Rader, J. N. Castañeda, J. R. Torczynski, and M. A. Gallis, Proceedings of the 26th International Symposium on Rarefied Gas Dynamics, 2008, Vol. 1084, p. 621.
[29] J. L. Xu and Z. Q. Zhou, Heat Mass Transfer **40**, 859 (2004).
[30] S. Maruyama, T. Kurashige, S. Matsumoto, Y. Yamaguchi, and T. Kimura, Nanoscale Microscale Thermophys. Eng. **2**, 49 (1998).
[31] S. Maruyama and T. Kimura, in *Fifth ASME/JSME Joint Thermal Engineering Conference* (ASME, San Diego, CA, 1999), p. 6511.
[32] K. Yamamoto, JSME Int. J. B. Fluid T **45**, 788 (2002).
[33] K. Yamamoto, H. Takeuchi, and T. Hyakutake, Proceedings of the 23rd International Symposium on Rarefied Gas Dynamics, 2003, Vol. 23, p. 1008.
[34] B.-Y. Cao, M. Chen, and Z.-Y. Guo, Appl. Phys. Lett. **86**, 091905 (2005).
[35] J. Sun and Z.-X. Li, Mol. Simul. **35**, 228 (2009).
[36] D. D. Do and H. D. Do, Fluid Phase Equilib. **236**, 169 (2005).
[37] H. Ambaye and J. R. Manson, Phys. Rev. E **73**, 031202 (2006).
[38] A. R. Leach, *Molecular Modelling-Principles and Applications*, 2nd ed. (Prentice Hall, Harlow, England, 2001).
[39] S. Y. Liem and K.-Y. Chan, Surf. Sci. **328**, 119 (1995).
[40] M. P. Allen and D. J. Tildesley, *Computer Simulation of Liquids*, 1st ed. (Oxford University Press, Oxford, England, 1987).
[41] P. G. de Gennes, Rev. Mod. Phys. **57**, 827 (1985).
[42] T. Werder, J. H. Walther, R. L. Jaffe, T. Halicioglu, and P. Koumoutsakos, J. Phys. Chem. B **107**, 1345 (2003).
[43] E. R. Cruz-Chu, A. Aksimentiev, and K. Schulten, J. Phys. Chem. B **110**, 21497 (2006).
[44] R. Tadmor, Langmuir **20**, 7659 (2004).
[45] T. Young, Philos. Trans. R. Soc. London, Ser. A **95**, 65 (1805).
[46] S. J. Kim, I. C. Bang, J. Buongiorno, and L. W. Hu, Appl. Phys. Lett. **89**, 153107 (2006).
[47] G. Saville, J. Chem. Soc., Faraday Trans. 2 **73**, 1122 (1977).
[48] J. H. Sikkenk, J. O. Indekeu, J. M. J. van Leeuwen, E. O. Vossnack, and A. F. Bakker, J. Stat. Phys. **52**, 23 (1988).
[49] M. J. P. Nijmeijer, C. Bruin, A. F. Bakker, and J. M. J. van Leeuwen, Phys. Rev. A **42**, 6052 (1990).
[50] J. H. Snoeijer and B. Andreotti, Phys. Fluids **20**, 057101 (2008).
[51] S. V. Nedea, A. J. Markvoort, A. A. van Steenhoven, and P. A. J. Hilbers, *Proceedings of the Fifth International Conference on Nanochannels, Microchannels and Minichannels* (ASME, Puebla, Mexico, 2007), p. 30039.
[52] P. Spijker, A. J. Markvoort, S. V. Nedea, and P. A. J. Hilbers, *Proceedings of the Sixth International Conference on Nanochannels, Microchannels and Minichannels* (ASME, Darmstadt, Germany, 2008), p. 62276.
[53] K. Yamamoto, H. Takeuchi, and T. Hyakutake, Phys. Fluids **19**, 087102 (2007).
[54] D. Bruno, M. Cacciatore, S. Longo, and M. Rutigliano, Chem. Phys. Lett. **320**, 245 (2000).
[55] P. Yi, D. Poulikakos, J. Walther, and G. Yadigaroglu, Int. J. Heat Mass Transfer **45**, 2087 (2002).
[56] D. Poulikakos, S. Arcidiacono, and S. Maruyama, Microscale Thermophys. Eng. **7**, 181 (2003).
[57] B.-Y. Cao, M. Chen, and Z.-Y. Guo, Phys. Rev. E **74**, 066311 (2006).
[58] M. Han, J. S. Lee, S. Park, and Y. K. Choi, Int. J. Heat Mass Transfer **49**, 879 (2006).
[59] C. S. Wang, J. S. Chen, J. Shiomi, and S. Maruyama, Int. J. Therm. Sci. **46**, 1203 (2007).
[60] G. Nagayama and P. Cheng, Int. J. Heat Mass Transfer **47**, 501 (2004).
[61] Y. S. Choi, S. J. Kim, and M.-U. Kim, Phys. Rev. E **73**, 016309 (2006).
[62] C. S. Kim, Trans. ASME **129**, 1140 (2007).
[63] N. Lümmen and T. Kraska, Nanotechnology **16**, 2870 (2005).
[64] F. Sharipov, Eur. J. Mech. B/Fluids **22**, 133 (2003).